HHS Public Access

Author manuscript

Magn Reson Med. Author manuscript; available in PMC 2017 August 18.

Published in final edited form as:

Magn Reson Med. 2016 December ; 76(6): 1677–1683. doi:10.1002/mrm.26457.

Quantitative Chemical Exchange Saturation Transfer MRI of Intervertebral Disc in a Porcine Model

Zhengwei Zhou[1,2,†], **Maxim Bez**[3,†], **Wafa Tawackoli**[1,4,5], **Joseph Giaconi**[6], **Dmitriy Sheyn**[4,5], **Sandra de Mel**[4,5], **Marcel M. Maya**[6], **Barry D. Pressman**[6], **Zulma Gazit**[3,4,5], **Gadi Pelled**[3,4,5], **Dan Gazit**[3,4,5], and **Debiao Li**[1,2,6,*]

[1]Biomedical Imaging Research Institute, Cedars-Sinai Medical Center, Los Angeles, California, USA

[2]Department of Bioengineering, University of California Los Angeles, Los Angeles, California, USA

[3]Skeletal Biotech Laboratory, The Hebrew University-Hadassah Faculty of Dental Medicine, Ein Kerem, Jerusalem, Israel

[4]Department of Surgery, Cedars-Sinai Medical Center, Los Angeles, California, USA

[5]Board of Governors Regenerative Medicine Institute, Cedars-Sinai Medical Center, Los Angeles, California, USA

[6]Department of Imaging, Cedars-Sinai Medical Center, Los Angeles, California, USA

Abstract

Purpose—Previous studies have associated low pH in interver-tebral discs (IVDs) with discogenic back pain. The purpose of this study was to determine whether quantitative CEST (qCEST) MRI can be used to detect pH changes in IVDs in vivo.

Methods—The exchange rate k_{sw} between glycosaminoglycan (GAG) protons and water protons was determined from qCEST analysis. Its dependence on pH value was investigated in GAG phantoms with varying pH and concentrations. The relationship between k_{sw} and pH was studied further in vivo in a porcine model on a 3T MR scanner and validated using a pH meter. Sodium lactate was injected into the IVDs to induce various pH values within the discs ranging from 5 to 7.

Results—Phantom and animal results revealed that k_{sw} measured using qCEST MRI is highly correlated with pH level. In the animal studies, the relationship can be described as $k_{sw} = 9.2 \times 10^6 \times 10^{-pH} + 196.9$, $R^2 = 0.7883$.

Conclusion—The exchange rate between GAG and water protons determined from qCEST MRI is closely correlated with pH value. This technique has the potential to noninvasively measure pH in the IVDs of patients with discogenic pain.

*Correspondence to: Debiao Li, Ph.D., Cedars-Sinai Medical Center, 8700 Beverly Boulevard, PACT Suite 800, Los Angeles, CA, 90048. debiao.li@cshs.org.

†These authors contributed equally to this work.

Keywords

intervertebral disc; low back pain; CEST; quantitative CEST; gagCEST; pH

INTRODUCTION

Lower back pain is a major medical condition estimated to affect up to 85% of the United States population (1). Intervertebral disc (IVD) degeneration is often associated with back pain. Although degenerate discs can be identified using MRI, they do not always cause pain. Therefore, if a patient with lower back pain has several degenerate discs, further examination is required to determine which disc is the source of the pain, prior to a decision of surgical intervention. Standard procedures include discography, during which the suspected discs are pressurized in order to provoke pain. This is a painful procedure that is also known to further accelerate disc degeneration, disc herniation, and loss of disc height and affect the adjacent endplates (2). It is also subjective to variations of the placement of the needle, pressure exerted, and anesthesia. Recent studies have associated low pH with discogenic pain (3,4). pH could potentially serve as a new metabolic biomarker for disco-genic back pain (5).

Chemical exchange saturation transfer (CEST) is an emerging MR technique to measure pH-dependent signal changes (6–9). This technique exploits the constant chemical exchange, which is pH-sensitive, between water protons and solute protons in certain molecules. The chemical exchange rate is dependent on pH values. The solute protons are first magnetization-saturated with a series of frequency-selective radiofrequency (RF) pulses, and after exchanging with water protons, the saturation is indirectly detected in the water signal (10,11).

Glycosaminoglycan (GAG) is a critical component to support the function in the IVD. It has been reported that GAG can be detected by CEST imaging because of its exchangeable hydroxyl protons (12,13). Previous studies have applied gagCEST to detect pH change in the IVD in animal models and patients with degenerative disc disease (14,15). However, CEST contrast is a rather complicated effect. It involves multiple confounding factors, including but not limited to 1) exchange rate between water and GAG protons, which is dependent on the pH; 2) labile proton ratio, which is linearly correlated with GAG concentration; 3) water relaxation parameters T_1 and T_2; and 4) the RF irradiation power of the CEST saturation module.

Multiple studies have focused on separating the exchange rate or the labile proton ratio from other confounding factors in the CEST experiments (16–21). Among these methods, quantitative CEST (qCEST) allows for simultaneous measurements of the exchange rate and labile proton ratio. It was developed based on the observation that the CEST effect can be represented as a linear function of $1/B_1^2$ (22). Multiple CEST experiments were performed with varying B_1 amplitudes for omega plot analysis (22).

Simultaneous measurements of pH value and concentration using qCEST have been shown in creatine phantom studies (18,20,21). Creatine protons have a slow to intermediate exchange rate with water protons (23). However, for GAG protons, which undergo relatively

faster chemical exchange, whether this technique can detect pH changes has not been investigated. In addition, most of the studies were performed on a preclinical scanner using continuous-wave saturation pulse (18,21). No in vivo validation has been performed and potential clinical application is not yet clear.

In this study, we propose an in vivo pH-dependent imaging technique in the IVD using qCEST on a 3T clinical scanner. We tested the technique in GAG phantoms and validated it in vivo in a porcine model using measurement from the tissue pH probe as reference.

THEORY

Previous investigators have studied the two-pool exchange model using Bloch-McConnell equations, describing the proton exchange between pool “w” (water pool) and pool “s” (solute pool). In this two-pool system, f_r refers to the labile proton ratio M_{0s}/M_{0w} and k_{sw} the exchange rate between solute pool and water pool. R_{1w}, R_{2w}, R_{1s}, and R_{2s} are longitudinal and transverse relaxation rates for water protons and solute protons, respectively.

The conventional CEST asymmetry analysis takes direct difference between the label scan (at the resonant frequency of the solute pool) and reference scan (at the opposite frequency with respect to water). It can be defined as $\mathrm{CESTR} = Z_{\mathrm{label}} - Z_{\mathrm{ref}}$, where Z_{label} and Z_{ref} are the normalized signal intensity or Z-spectrum for the label scan and reference scan. However, this analysis has its limits with regard to quantitative imaging, because its expression is rather complicated and involves multiple confounding factors.

In recent studies, the inverse CEST difference ($\mathrm{CES\text{-}TR_{ind}}$) was proposed because of its simplified expression (16,18)

$$\frac{1}{\mathrm{CESTR_{ind}}}=\frac{1}{\frac{1}{Z_{\mathrm{label}}}-\frac{1}{Z_{\mathrm{ref}}}}\approx\frac{R_{1w}}{f_r\cdot k_{sw}}+\frac{k_{sw}\cdot(R_{2s}+k_{sw})\cdot R_{1w}}{f_r\cdot k_{sw}}\frac{1}{\omega_1^2}, \quad [1]$$

where ω_1 is the RF irradiation amplitude.

Equation [1] is only valid for continuous-wave CEST saturation. When pulsed saturation is applied in CEST experiments, Eq. [1] can be written as (20)

$$\frac{1}{\mathrm{CESTR_{ind}}}\approx\frac{R_{1w}}{DC\cdot f_r\cdot k_{sw}\cdot c_1}+\frac{k_{sw}\cdot(R_{2s}+k_{sw})\cdot R_{1w}\cdot c_2^2}{DC\cdot f_r\cdot k_{sw}\cdot c_1}\frac{1}{\omega_1^2}, \quad [2]$$

where DC represents the duty cycle and c_1 and c_2 represent the shape of Gaussian saturation pulses ($c_1=\sigma\sqrt{2\pi}/t_p$, $c_2=c_1\sqrt{\sqrt{2}}$; σ and t_p are the width and length of the Gaussian pulse). Note that ω_1 here is defined as the average RF irradiation amplitude of one Gaussian pulse (i.e., ω_1 = flip angle/pulse duration). This equation is equivalent to Equation 18 by Meissner et al. (20).

In this expression, $1/CESTR_{ind}$ is described as a linear function of $1/\omega_1^2$. By measuring $CESTR_{ind}$ with different RF irradiation amplitude, we can calculate the slope m and intercut n and eventually estimate k_{sw} and f_r:

$$k_{sw}=\frac{\sqrt{R_{2s}^2+\frac{4m}{n\cdot c_2^2}}-R_{2s}}{2} \quad [3]$$

$$f_r=\frac{R_{1w}}{k_{sw}\cdot n\cdot c_1\cdot DC} \quad [4]$$

R_{1w} can be measured using T_1 mapping techniques. R_{2s} of GAG is approximately 200 s^{-1} (24).

Note that Eq. [1] is a simplified expression that describes the steady state signal of CEST imaging. When performing qCEST experiments, RF saturation pulses need to be long enough to ensure the steady state is reached. The simplification only holds for dilute CEST agents undergoing slow and intermediate chemical exchange.

METHODS

Phantom

Two sets of phantoms containing GAG prepared from chondroitin sulphate A (Sigma-Aldrich, St. Louis, Missouri, USA) and phosphate-buffered saline with varying pH values and concentrations were prepared. For the pH set, the GAG concentration was fixed at 60 mM and pH was titrated to 5.8, 6.1, 6.4, 6.7, and 7.0. For the concentration phantom, we used various GAG concentrations (100, 80, 60, 40, and 20 mM) and titrated the pH to 7.0. The solution was then transferred to 15 mL tubes. These 10 tubes were put in a phantom holder filled with water.

In Vitro MRI Experiments

Imaging experiments were performed at room temperature on a 3T clinical scanner (Magnetom Verio; Siemens Healthcare, Erlangen, Germany). All images were acquired with a slice thickness of 8 mm, field of view of 160 × 160 mm^2, and imaging matrix of 128 × 128.

CEST MRI was performed with pulsed RF saturation turbo spin echo (TSE) sequence (pulse repetition time [TR]/echo time [TE] = 16,000/12 ms; two averages). The CEST saturation module consisted of 39 Gaussian-shaped pulses, with a duration t_p =80 ms for each pulse and an interpulse delay t_d = 80 ms (duty cycle = 50%, total saturation time T_{sat} = 6240 ms) at saturation flip angle 900°, 1500°, 2100°, and 3000° [B_1 amplitudes = flip angle/(γt_p) = 0.73, 1.22, 1.71, and 2.45 μT; Gaussian saturation pulse parameters c_1 = 0.50, c_2 = 0.59]. Z-spectrum was acquired with 10 different saturation frequencies at ±1.6, ±1.3, ±1.0, ±0.7, and

±0.4 ppm. The B_0 field was corrected using a water saturation shift referencing (WASSR) map (25).

T_1-weighted MR images were acquired by an inversion recovery TSE sequence with 10 different inversion delays (inversion time [TI] =50, 150, 350, 700, 1050, 1400, 2000, 2500, 3000, and 4000 ms; TR/TE=6000/12 ms). T_2-weighted MR images were acquired using a TSE sequence with varying echo delays (TE = 12, 24, 48, 97, 205, and 399 ms; TR = 6000 ms).

Animal Preparation

All animal-related procedures were approved by the Institutional Animal Care and Use Committee at Cedars-Sinai Medical Center. Four female Yucatan minipigs (S&S Farms, Ramona, California, USA) were used. Following an 18-hour preoperative fast, the pigs were sedated with intramuscular drugs (acepromazine 0.25 mg/kg, ketamine 20 mg/kg, and atropine 0.02–0.05 mg/kg) and were then injected intravenously with propofol (2 mg/kg) to induce full anesthesia. The trachea was intubated and anesthesia was maintained using 1%–3.5% isoflurane inhaled via the tracheal tube for the duration of the procedure. Under fluoroscopic guidance, three MR-compatible 14G coaxial needles (Invivo, Gainesville, Florida, USA) were inserted into the mid-substance of lumbar discs L1/L2, L3/L4, and L5/L6. These lumbar discs were injected with different concentrations of sodium lactate (Sigma-Aldrich) in order to induce a gradient of pH values within the discs ranging from 5 to 7, as described by Melkus et al. (15) and in accordance with pH values measured within patients' pathological discs (26). After intradiscal injection, exact pH values inside the discs were measured using a custom-made needle-shaped tissue pH probe (Warner Instruments, Hamden, Connecticut, USA) which was inserted through the MR-compatible needle shortly before the MR scan. Lumbar disc L2/L3 was also scanned as the control disc. Its pH value was measured immediately after the animal was euthanized.

In Vivo MRI Experiments

Imaging experiments were performed on a 3T clinical scanner (Magnetom Verio; Siemens Healthcare, Erlangen, Germany). Animals were placed in the right decubitus position with body array coils centered on the posterior aspect spinous process. Throughout the imaging procedures, anesthesia was maintained with isoflurane (1%–3.5%).

CEST MRI was performed using a two-dimensional reduced field of view TSE CEST sequence (TR/TE = 10,500/10 ms, two averages, single shot). Reduced field of view can effectively suppress bowel motion artifacts and increase scan efficiency (27). For each IVD, images were acquired in the axial plane with a slice thickness of 3 mm, field of view of 100 × 40 mm^2, and spatial resolution of 0.8 × 0.8 mm^2. CEST saturation module consists of 39 Gaussian-shaped pulses, with a duration t_p = 80 ms for each pulse and an interpulse delay t_d = 80 ms (duty cycle = 50%, total saturation duration T_s = 6240 ms) at saturation flip angle 900°, 1500°, 2100°, and 3000° [B_1 amplitudes = flip angle/(γt_p) = 0.73, 1.22, 1.71, and 2.45 μT; Gaussian saturation pulse parameters c_1 = 0.50, c_2 = 0.59]. Z-spectrum was acquired with 10 different saturation frequencies at ±1.6, ±1.3, ±1.0, ±0.7, and ±0.4 ppm. The scan

time of the CEST experiment for each RF irradiation amplitude was approximately 6 min. The B_0 field was corrected using WASSR.

T_1-weighted MR images were acquired using an inversion recovery TSE sequence with seven varying TI (50, 150, 350, 700, 1050, 1400, and 2000 ms). Images were acquired at the same slice position as the CEST MRI sequence (TR/TE = 6000/12 ms; 1 average; FOV = 200 × 200 mm^2; spatial resolution = 0.8 × 0.8 × 3 mm^3; scan time = ~2.5 min).

Data Analysis

Postprocessing was performed with custom-written programs in MATLAB (MathWorks, Natick, Massachusetts, USA). $CESTR_{ind}$ was calculated according to Eq. [1] after B_0 correction at 1.0 ppm [Z_{lab} = Z(+1.0 ppm), Z_{ref} = Z(−1.0 ppm)]. Linear regression was used to perform Ω-plot analysis between 1/$CESTR_{ind}$ and $1/\omega_1^2$ to obtain the slope and intercut. The exchange rate k_{sw} and labile proton ratio f_r were calculated afterward following Eqs. [3] and [4]. These calculations were performed pixel-by-pixel and by region of interest (ROI). The T_1 maps were obtained by pixel-by-pixel least-squares fitting of the signal equation $I = I_0[1 - (1 + \eta) \cdot \exp(-TI/T_1)]$, where I is the signal intensity, TI is the inversion time, and η is the inversion efficiency. The T_2 maps were obtained by fitting the signal equation $I = I_0 \cdot \exp(-TE/T_2)]$, where I is the signal intensity and TE is the echo time.

RESULTS

Phantom

In Figure 1, we evaluated the relationship between 1/CES-TR_{ind} and $1/\omega_1^2$ in tubes with varying GAG concentration and pH values. 1/$CESTR_{ind}$ is the average signal within the region-of-interest (ROI) of each tube. In all tubes, 1/$CESTR_{ind}$ can be represented as a linear function of $1/\omega_1^2$. This experimental finding is consistent with Eq. [2].

In addition, pixel-wise mapping of chemical exchange rate k_{sw} and labile proton ratio f_r were reconstructed (Fig. 2). One can appreciate the dependence of chemical exchange rate on pH (Fig. 2a) and labile proton ratio on GAG concentrations (Fig. 2b). Quantitatively, the chemical exchange rate can be described as $k_{sw} = 1.5 \times 10^8 \times 10^{-pH} + 252.0$, $R^2 = 0.9508$ (Fig. 2c). This follows an acid catalyzed chemical exchange formula (28). The labile proton ratio is linearly correlated with GAG concentration (Fig. 2d). It can be represented as $f_r = 4.6 \times 10^{-5}$ [GAG] − 4.4×10^{-5}($R^2 = 0.9869$), where [GAG] is the GAG concentration in mM. The error bars in Figure 2c and 2d represent the standard deviation of all the pixels within the ROI of each tube for k_{sw} and f_r, respectively. These experimental results encouraged in vivo application of qCEST technique.

Animal Studies

Sixteen IVDs were investigated in this study, three of which were excluded because the needle went through both sides of the IVD and caused morphological damage. The pH values of the studied IVDs after sodium lactate injection ranged from 5.0 to 7.2.

Figure 3 shows the anatomical images of one representative pig's lumbar IVDs and the corresponding exchange rate maps. As shown in the figure, the exchange rate was higher in the IVDs with lower pH values. Within each disc, there was some inhomogeneity in the exchange rate map. This is partially because at the current SNR, we cannot guarantee accurate measurement for a signal pixel. However, the average value within the ROI of each IVD will provide more reliable measurement. This is because the SNR will increase after averaging all pixels that are in the similar pH environment.

As shown in Figure 4a, we evaluated the relationship between $1/\mathrm{CESTR}_{\mathrm{ind}}$ and $11/\omega_1^2$ in representative IVDs with different pH values (5.0, 5.8, and 6.7). Similar to the phantom studies, $1/\mathrm{CESTR}_{\mathrm{ind}}$ can be represented as a linear function of $1/\omega_1^2$. In Figure 4b, we took the average exchange rate of each disc and evaluated its relationship with the corresponding pH value, which was obtained by directly measuring the intradiscal pH value using a pH probe. The exchange rate can be described by an acid catalyzed chemical exchange formula $k_{sw} = 9.2 \times 10^6 \times 10^{-\mathrm{pH}} + 196.9$, $R^2 = 0.7883$. However, because of the difficulty in determining the location of the pH probe, there could be some uncertainty of the pH values measured by the tissue pH probe.

DISCUSSION

In this study, we investigated the feasibility of qCEST technique to detect pH changes in IVDs in vivo on a 3T MR scanner. Phantom studies showed that the approximations used in qCEST analysis hold true for GAG and that the exchange rate determined from qCEST analysis is dependent on pH levels of GAG solutions. The relationship between the exchange rate and pH was further studied in the porcine spine studies. The results showed the exchange rate can be described as a function of pH using acid catalyzed proton chemical exchange formula. To our knowledge, this is the first in vivo study to show the validity of qCEST analysis using tissue pH meter as reference.

Previous studies have investigated the pH dependence of gagCEST. Even though the GAG concentration can be corrected using $T_{1\rho}$, water relaxation parameters T_1 and T_2 still contribute to the gagCEST signal (14). qCEST analysis, on the other hand, has been shown to detect pH changes independent of T_1, T_2, and concentration in numerical simulations and in phantom studies (18,20). It is a more reliable approach to measure pH changes in the IVD, because T_1 and T_2 change significantly after disc degeneration (29). In the present in vivo study, we established a relationship between exchange rates and pH levels, which can be potentially applied in future studies to translate exchange rates to pH levels.

Pulsed CEST saturation pulses were used because this study was performed on a 3T clinical MR scanner. Pulsed qCEST analysis is even more complicated because of the constantly changing RF irradiation amplitude. Pulsed CEST experiments normally report the irradiation power as the equivalent continuous-wave B_1 field strength. However, the proton exchange in pulsed CEST experiments is rather complicated. Simply integrating the equivalent continuous-wave B_1 field strength will cause errors in estimating the exchange rate and labile proton ratio. Meissner et al. (20) developed an analytical solution for pulsed CEST experiment. This enables more accurate quantitative results of pulsed CEST experiments.

It should be noted that because of the simplification of the in vivo situation, there could be some potential systemic error in estimating the exchange rate. One error source is magnetization transfer effects are not considered. This will lead to the underestimation of CEST effects, especially when the RF irradiation amplitude is higher, which means the slope can be also underestimated. Therefore, there could be underestimation of exchange rate when magnetization transfer effects are not considered. Another error source is the approximation of the Gaussian-shaped saturation pulses. Even though we have made some corrections as discussed above, the performance of the Gaussian-shaped pulses is not fully simulated, especially in the case of intermediate to fast chemical exchange.

In this study, we explored the relationship between exchange rates and pH levels in both phantom studies and in vivo animal studies. However, the results are not exactly the same. One reason is these two studies were performed at different temperatures (~20°C for phantom studies and ~38°C for animal studies). Another possible reason is the GAG protons in the IVD experience a more complicated environment. In addition to CEST effects, magnetization transfer effects are also present in the IVD from semisolid components such as macromolecules, which could affect the qCEST analysis (16). As discussed above, because we did not consider magnetization transfer effects in our model, there is systemic error of underestimating the exchange rate in the in vivo studies, which explains the discrepancy between phantom and animal studies.

A potential limitation of this study is the long scan time (30–40 min for one IVD). Regular CEST experiments are relatively slow because of long TR, multiple averages, and so forth. In addition, qCEST analysis requires 1) long RF saturation time (6 s in our study) to achieve the steady state and 2) multiple CEST experiments with varying RF irradiation amplitudes to perform the Ω-plots. Compressed sensing and parallel imaging techniques can be used to accelerate qCEST experiments (30).

It is known that CEST imaging is prone to B_1 inhomogeneity. Not knowing the exact B_1 field may cause errors in the estimation of exchange rate k_{sw}. We performed a pilot study and found that the B_1 field is relatively homogenous within the small ROI (nucleus pulposus) for all discs; this is why we did not acquire a B_1 map for every IVD. It should be noted though, that B_1 inhomogeneity issues need to be carefully considered in qCEST imaging to avoid potential errors.

The manipulation of pH levels in the IVDs by injecting sodium lactate mimics the degeneration condition only to a limited extent. In addition to pH change, disc degeneration is also correlated with a loss of GAG and water content in the nucleus pulposus (31). GAG loss will significantly lower the CEST values (32), and the dehydration process will cause a change of MR relaxation parameters (33,34). In order to better simulate the degeneration situation, qCEST experiments could be performed in the disc degenerative porcine model (35) and in patients with discogenic pain (14).

CONCLUSIONS

Our work demonstrates the feasibility of in vivo qCEST analysis of GAG in IVDs. The validation study shows that the exchange rate determined from qCEST analysis is closely correlated with pH value, and can be used to noninvasively measure pH in IVDs. qCEST technique has the potential to provide additional information on IVD physiology and help gain insight into the pathogenesis of low back pain and its underlying degenerative processes.

Acknowledgments

We thank Phillip Zhe Sun for helpful discussion. We also thank Edward Gill, Laura G. Smith, Hernan Rios, and Richard Tang for help conducting the imaging experiments.

Grant sponsor: National Institute of Arthritis and Musculoskeletal and Skin Diseases; Grant number: R01AR066517.

Zulma Gazit, Gadi Pelled, and Dan Gazit are founders and equity holders in TavorStem Therapeutics. TavorStem Therapeutics provided no funding for this study.

References

1. Knox J, Orchowski J, Scher DL, Owens BD, Burks R, Belmont PJ. The incidence of low back pain in active duty United States military service members. Spine. 2011; 36:1492–1500. [PubMed: 21224777]
2. Carragee EJ, Don AS, Hurwitz EL, Cuellar JM, Carrino JA, Carrino J, Herzog R. 2009 ISSLS prize winner: does discography cause accelerated progression of degeneration changes in the lumbar disc: a ten-year matched cohort study. Spine. 2009; 34:2338–2345. [PubMed: 19755936]
3. Liang C-Z, Li H, Tao Y-Q, Zhou X-P, Yang Z-R, Li F-C, Chen Q-X. The relationship between low pH in intervertebral discs and low back pain: a systematic review. Arch Med Sci. 2012; 8:952–956. [PubMed: 23319966]
4. Liang C, Li H, Tao Y, Shen C, Li F, Shi Z, Han B, Chen Q. New hypothesis of chronic back pain: low pH promotes nerve ingrowth into damaged intervertebral disks. Acta Anaesthesiol Scand. 2013; 57:271–277. [PubMed: 22404297]
5. Keshari KR, Lotz JC, Link TM, Hu S, Majumdar S, Kurhanewicz J. Lactic acid and proteoglycans as metabolic markers for discogenic back pain. Spine. 2008; 33:312–317. [PubMed: 18303465]
6. Zhou J, Payen J-F, Wilson DA, Traystman RJ, van Zijl PCM. Using the amide proton signals of intracellular proteins and peptides to detect pH effects in MRI. Nat Med. 2003; 9:1085–1090. [PubMed: 12872167]
7. Sun PZ, Murata Y, Lu J, Wang X, Lo EH, Sorensen AG. Relaxation-compensated fast multislice amide proton transfer (APT) imaging of acute ischemic stroke. Magn Reson Med. 2008; 59:1175–1182. [PubMed: 18429031]
8. Sun PZ, Zhou J, Sun W, Huang J, van Zijl PCM. Detection of the ischemic penumbra using pH-weighted MRI. J Cereb Blood Flow Metab. 2007; 27:1129–1136. [PubMed: 17133226]
9. Zhou J, van Zijl PCM. Defining an acidosis-based ischemic penumbra from pH-weighted MRI. Transl Stroke Res. 2011; 3:76–83. [PubMed: 22408691]
10. van Zijl PCM, Yadav NN. Chemical exchange saturation transfer (CEST): what is in a name and what isn't? Magn Reson Med. 2011; 65:927–948. [PubMed: 21337419]
11. Ward KM, Aletras AH, Balaban RS. A new class of contrast agents for MRI based on proton chemical exchange dependent saturation transfer (CEST). J Magn Reson. 2000; 143:79–87. [PubMed: 10698648]
12. Ling W, Regatte RR, Navon G, Jerschow A. Assessment of glycosami-noglycan concentration in vivo by chemical exchange-dependent saturation transfer (gagCEST). Proc Natl Acad Sci U S A. 2008; 105:2266–2270. [PubMed: 18268341]

13. Saar G, Zhang B, Ling W, Regatte RR, Navon G, Jerschow A. Assessment of glycosaminoglycan concentration changes in the interverte-bral disc via chemical exchange saturation transfer. NMR Biomed. 2012; 25:255–261. [PubMed: 22253087]
14. Liu Q, Tawackoli W, Pelled G, et al. Detection of low back pain using pH level-dependent imaging of the intervertebral disc using the ratio of R1ρ dispersion and-OH chemical exchange saturation transfer (RROC). Magn Reson Med. 2015; 73:1196–1205. [PubMed: 24700573]
15. Melkus G, Grabau M, Karampinos DC, Majumdar S. Ex vivo porcine model to measure pH dependence of chemical exchange saturation transfer effect of glycosaminoglycan in the intervertebral disc. Magn Reson Med. 2014; 71:1743–1749. [PubMed: 23818244]
16. Zaiss M, Xu J, Goerke S, Khan IS, Singer RJ, Gore JC, Gochberg DF, Bachert P. Inverse Z-spectrum analysis for spillover-, MT-, and T1 - corrected steady-state pulsed CEST-MRI-application to pH-weighted MRI of acute stroke. NMR Biomed. 2014; 27:240–252. [PubMed: 24395553]
17. Sun PZ, Wang Y, Dai Z, Xiao G, Wu R. Quantitative chemical exchange saturation transfer (qCEST) MRI—RF spillover effect-corrected omega plot for simultaneous determination of labile proton fraction ratio and exchange rate. Contrast Media Mol Imaging. 2014; 9:268–275. [PubMed: 24706610]
18. Wu R, Xiao G, Zhou IY, Ran C, Sun PZ. Quantitative chemical exchange saturation transfer (qCEST) MRI—omega plot analysis of RF-spillover-corrected inverse CEST ratio asymmetry for simultaneous determination of labile proton ratio and exchange rate. NMR Biomed. 2015; 28:376–383. [PubMed: 25615718]
19. Wu R, Longo DL, Aime S, Sun PZ. Quantitative description of radio-frequency (RF) power-based ratiometric chemical exchange saturation transfer (CEST) pH imaging. NMR Biomed. 2015; 28:555–565. [PubMed: 25807919]
20. Meissner J-E, Goerke S, Rerich E, Klika KD, Radbruch A, Ladd ME, Bachert P, Zaiss M. Quantitative pulsed CEST-MRI using Ω-plots. NMR Biomed. 2015; 28:1196–1208. [PubMed: 26278686]
21. Sun PZ, Xiao G, Zhou IY, Guo Y, Wu R. A method for accurate pH mapping with chemical exchange saturation transfer (CEST) MRI. Contrast Media Mol Imaging. 2016; 11:195–202. [PubMed: 26689424]
22. Dixon WT, Ren J, Lubag AJM, Ratnakar J, Vinogradov E, Hancu I, Lenkinski RE, Sherry AD. A concentration-independent method to measure exchange rates in PARACEST agents. Magn Reson Med. 2010; 63:625–632. [PubMed: 20187174]
23. Haris M, Nanga RPR, Singh A, Cai K, Kogan F, Hariharan H, Reddy R. Exchange rates of creatine kinase metabolites: feasibility of imaging creatine by chemical exchange saturation transfer MRI. NMR Biomed. 2012; 25:1305–1309. [PubMed: 22431193]
24. Lee J-S, Xia D, Jerschow A, Regatte RR. In vitro study of endogenous CEST agents at 3 T and 7 T. Contrast Media Mol Imaging. 2016; 11:4–14. [PubMed: 26153196]
25. Kim M, Gillen J, Landman BA, Zhou J, van Zijl PCM. Water saturation shift referencing (WASSR) for chemical exchange saturation transfer (CEST) experiments. Magn Reson Med. 2009; 61:1441–1450. [PubMed: 19358232]
26. Nachemson A. Intradiscal measurements of pH in patients with lumbar rhizopathies. Acta Orthop Scand. 1969; 40:23–42. [PubMed: 4312806]
27. Liu Q, Jin N, Fan Z, Natsuaki Y, Tawackoli W, Pelled G, Bae H, Gazit D, Li D. Reliable chemical exchange saturation transfer imaging of human lumbar intervertebral discs using reduced-field-of-view turbo spin echo at 3.0 T. NMR Biomed. 2013; 26:1672–1679. [PubMed: 23893565]
28. Englander SW, Downer NW, Teitelbaum H. Hydrogen exchange. Annu Rev Biochem. 1972; 41:903–924. [PubMed: 4563445]
29. Antoniou J, Pike GB, Steffen T, Baramki H, Poole AR, Aebi M, Alini M. Quantitative magnetic resonance imaging in the assessment of degenerative disc disease. Magn Reson Med. 1998; 40:900–907. [PubMed: 9840835]
30. Heo HY, Zhang Y, Lee DH, Jiang S, Zhao X, Zhou J. Accelerating chemical exchange saturation transfer (CEST) MRI by combining compressed sensing and sensitivity encoding techniques. Magn Reson Med. 2016; doi: 10.1002/mrm.26141

31. An HS, Anderson PA, Haughton VM, Iatridis JC. Introduction: disc degeneration: summary. Spine. 2004; 29:2677–2678. [PubMed: 15564916]

32. Haneder S, Apprich SR, Schmitt B, Michaely HJ, Schoenberg SO, Friedrich KM, Trattnig S. Assessment of glycosaminoglycan content in intervertebral discs using chemical exchange saturation transfer at 3.0 Tesla: preliminary results in patients with low-back pain. Eur Radiol. 2013; 23:861–868. [PubMed: 23052643]

33. Takashima H, Takebayashi T, Yoshimoto M, Terashima Y, Tsuda H, Ida K, Yamashita T. Correlation between T2 relaxation time and intervertebral disk degeneration. Skeletal Radiol. 2012; 41:163–167. [PubMed: 21424906]

34. Wang Y-XJ, Zhao F, Griffith JF, Mok GSP, Leung JCS, Ahuja AT, Yuan J. T1rho and T2 relaxation times for lumbar disc degeneration: an in vivo comparative study at 3.0-Tesla MRI. Eur Radiol. 2013; 23:228–234. [PubMed: 22865227]

35. Kim KS, Yoon ST, Li J, Park JS, Hutton WC. Disc degeneration in the rabbit: a biochemical and radiological comparison between four disc injury models. Spine. 2005; 30:33. [PubMed: 15626978]

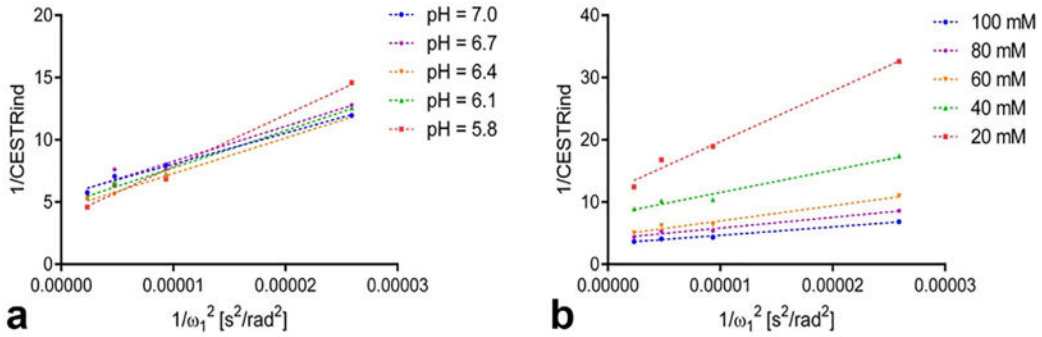

FIG. 1.

Ω-plots analysis of (a) phantoms with the same concentration (60 mM) but varying pH values (5.8, 6.1, 6.4, 6.7, and 7.0) and (b) phantoms with the same pH value (7.0) but varying GAG concentrations (20, 40, 60, 80, and 100 mM).

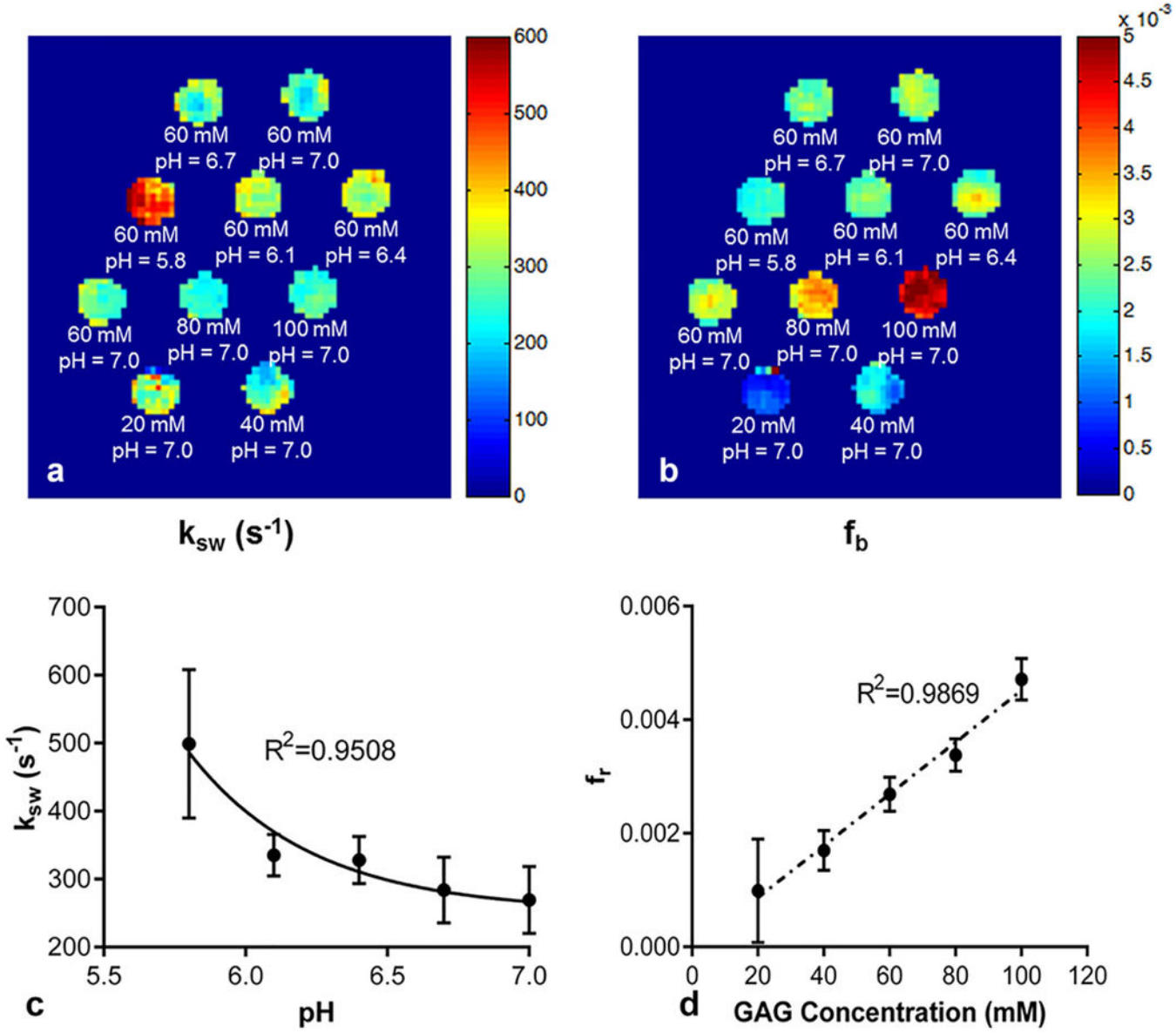

FIG. 2.

Quantitative results of the phantom study. (**a**) Pixel-wise mapping of labile proton exchange rate. (**b**) Pixel-wise mapping of labile proton ratio. (**c**) Chemical exchange rate as a function of pH. (**d**) Labile proton ratio as a function of GAG concentration. The error bars in panels (c) and (d) represent the standard deviation of all the pixels within the ROI of each tube for k_{sw} and f_r, respectively.

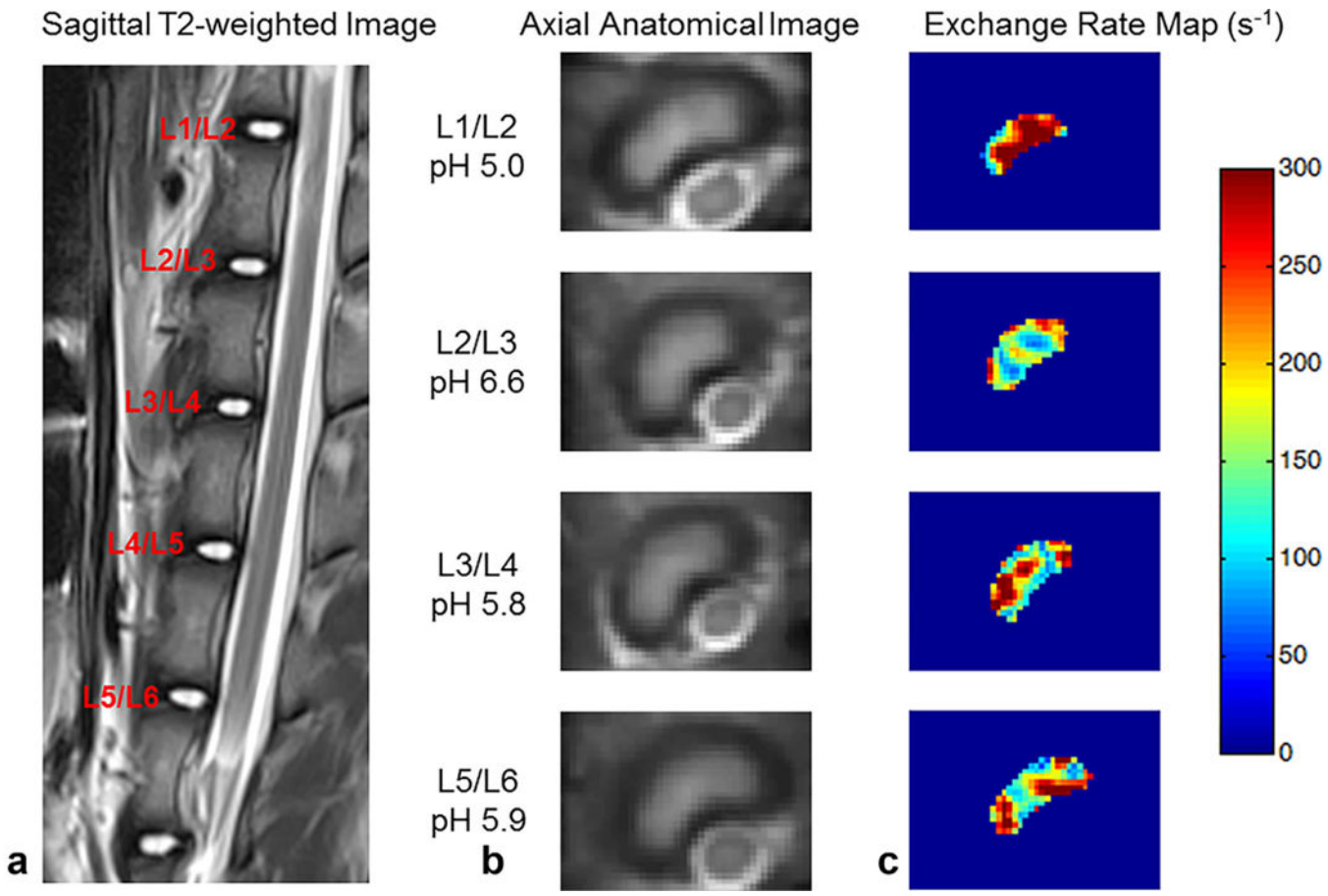

FIG. 3.

Representative images of IVDs and corresponding exchange rate maps in one pig. (**a**) T_2-weighted image in the sagittal plane. (**b**) Axial anatomical images of corresponding IVDs. (**c**) Exchange rate maps of corresponding IVDs. The IVDs with lower pH tend to have a higher exchange rate.

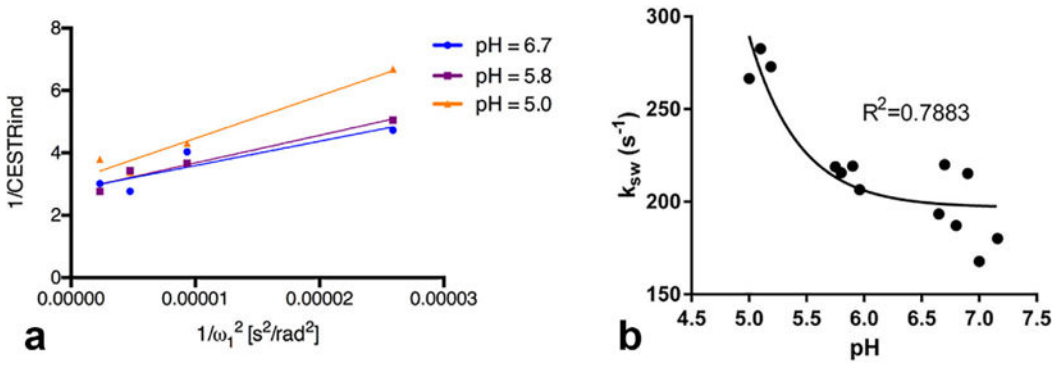

FIG. 4.

(a) Ω-plot analysis of representative IVDs with varying pH values (5.0, 5.8, and 6.7). (b) Cchemical exchange rate as a function of pH in the animal studies.